

# Entanglement entropy of higher rank topological phases

Hiromi Ebisu<sup>1</sup>

<sup>1</sup>*Department of Physics and Astronomy,  
Rutgers University, Piscataway, NJ 08854, USA*

(Dated: February 23, 2023)

## Abstract

We study entanglement entropy of unusual  $\mathbb{Z}_N$  topological stabilizer codes which admit fractional excitations with restricted mobility constraint in a manner akin to fracton topological phases. It is widely known that the sub-leading term of the entanglement entropy of a disk geometry in conventional topologically ordered phases is related to the total number of the quantum dimension of the fractional excitations. We show that, in our model, such a relation does not hold, i.e, the total number of the quantum dimension varies depending on the system size, whereas the sub-leading term of the entanglement entropy takes a constant number irrespective to the system size. We give a physical interpretation of this result in the simplest case of the model.

## CONTENTS

I. Introduction	3
II. Stabilizer model	4
A. Hamiltonian	5
B. Simplest case: $N = 2$	6
C. Logical operators and Ground state degeneracy	8
III. Entanglement entropy	13
A. Review of the bipartite entanglement in lattice spin systems	14
1. Reduced density matrix	14
2. Entanglement entropy of a subsystem	15
B. Single-row/column geometry	15
1. Single row I	17
2. Single row II	17
3. Single column	18
C. Disk geometry	19
IV. Alternative interpretation of the result in the simplest case	24
V. Brief comments on other cases of the higher rank topological phases	25
VI. Conclusion	27
Acknowledgement	28
References	28
A. Proof of Eq. (37)	29
B. Entanglement entropy with respect to the generic ground state	30
1. Single row I	30
2. Single row II	31
3. Single column	32

## I. INTRODUCTION

Quantum entanglement is one of the central subjects in contemporary physics [1, 2]. It has shed new lights on various fields of physics, such as quantum information, condensed matter physics, and high energy physics. For instance, the entanglement entropy has been intensively studied in various systems [3] and it was found that it exhibits the unique scaling dependence on the system size [4–6]. Remarkably, in some cases, it extracts a universal number, such as central charge which appears as the coefficient of the leading term [7–9]. In topological phases of matter (see the next paragraph for more explanation), the sub-leading part of the entanglement entropy contains universal properties of topological orders in the system [10, 11]. Also, quantum entanglement plays a pivotal role in understanding quantum gravity in view of holography [12–17].

In this paper, we focus on the quantum entanglement in new type of topological stabilizer codes by studying entanglement entropy. Topological stabilizer codes fall into the category of topologically ordered phases in the context of condensed matter physics [18–21], which have drawn a lot of attention for decades due to the fact that these phases carry exotic fractionalized excitations namely anyons [22, 23]. In application perspective, these excitations are expected to be utilized for implementing quantum computers. In particular, these phases have been thoroughly studied in view of quantum error correcting codes [24–26].

A plethora of progress has been made in understanding quantum entanglement of these phases. It is well known that the entanglement entropy of the 2D topologically ordered phases in the disk bipartite geometry  $A$ ,  $S_A$  scales as [10, 11]

$$S_A \sim \alpha l - \gamma + \dots \quad (1)$$

The first term, which is the leading term, is the so-called area-law term, proportional to the perimeter of the disk geometry  $l$  with  $\alpha$  being non-universal constant, whereas the second constant term, which is the sub-leading term, is of particularly importance as it is universal number, referred to as the *topological entanglement entropy*. It is rewritten as

$$\gamma = \log \left( \sqrt{\sum_a d_a^2} \right), \quad (2)$$

where  $d_a$  represents the quantum dimension of the anyon labeled by  $a$ . [ $\dots$  in (1) represents terms that vanish in the limit of  $l \rightarrow \infty$ .]

While a lot of theoretical and experimental efforts have been devoted to elucidate these phases, recently, a new type of topologically ordered phases have been proposed, so-called fracton topological phases [27–29]. The distinctive property of these phases is that the fractional excitations are

subject to the mobility constraint, giving rise to the sub-extensive ground state degeneracy (GSD). This can be intuitively understood by that the excitations are sensitive to the local geometry of the system. Since the phase is sensitive to the UV physics, one cannot have proper theoretical framework to classify these phases based on topology. From this reason, understanding these phases has yet to be completed.

Previously, we introduced a simple exactly solvable  $\mathbb{Z}_N$  stabilizer model in 2D [30], which hosts the fractional excitations with the similar mobility constraint as the fracton topological phases, yielding unusual dependence of the GSD on the system size. The aim of this paper is to explore interplay between entanglement entropy and the model studied in [30]. We investigate entanglement entropy of various geometries of the subsystems. In particular, we study the entanglement entropy of the disk geometry. By making use of the formalism of the entanglement entropy for stabilizer codes [31], jointly with the one in the graph theory, we show that the entanglement entropy is described by the same form as (1), yet Eq. (2), which is an important relation between entanglement entropy and the total quantum dimension of fractional excitations, does *not* hold. Indeed, while the total quantum dimension varies depending on the geometry of the lattice, the topological entanglement entropy  $\gamma$  takes the constant number, irrespective to the lattice. We give an intuitive interpretation of the result by focusing on the simplest case by setting  $N = 2$ . Our results are summarized in Table. I.

The rest of the paper is organized as follows. In Sec. II, we review the model and its properties studied in [30]. After reviewing the model, in Sec. III, we calculate entanglement entropy of various geometries of subsystems. In Sec. IV, we give an intuitive understanding of our result on the entanglement entropy. We make a brief comment on other cases of topological phases in Sec. V. Finally, we conclude our work in Sec. VI. Technical details are relegated to appendices.

## II. STABILIZER MODEL

In this section, we review the model constructed by stabilizers given in [30]. Also, we go over physical properties of the model. As we mentioned in the previous section, the model exhibits unusual behavior of the excitations compared with the conventional topologically ordered phases, yielding the unusual GSD dependence on the lattice.

### A. Hamiltonian

To start, we introduce 2D square lattice where we place two types of  $N$ -qubit state ( $\mathbb{Z}_N$  clock states) on each vertex and vertical link. The first clock states are located at vertices of the lattice whereas the second ones are at vertical links. We label the coordinate of the first clock states by  $(x, y)$  and the ones of the second clock states are denoted by  $(x, y + \frac{1}{2})$ , where the second element corresponds to the links between vertices located at  $(x, y)$  and  $(x, y + 1)$ . We term these two types of the clock states clock state with type 1 and clock state with type 2.

We represent basis of the two types of the clock states as  $|\omega\rangle_1$  and  $|\omega\rangle_2$  with  $\omega$  being  $N$ -th root of unity, i.e.,  $\omega = e^{2\pi i/N}$  [red square and blue dot in Fig. 1(a)], and  $\mathbb{Z}_N$  shift and clock operators (they become Pauli operators when  $N = 2$ ) of the first and second clock states as  $\{Z_i, X_i\}$  ( $i = 1, 2$ ). Here we have introduced the subscript  $i = 1, 2$  to distinguish operators that act on the clock clock states with type 1 and the ones with type 2. These operators satisfy the following relation ( $I_i$  denotes the identity operator)

$$X_i^N = Z_i^N = I_i, \quad Z_i |\omega\rangle_i = \omega |\omega\rangle_i, \quad X_i Z_j = \omega Z_j X_i \delta_{i,j}. \quad (3)$$

With these notations, we define following two types of operators at each vertex and link

$$\begin{aligned} V_{(x,y)} &:= X_{2,(x,y+1/2)} X_{2,(x,y-1/2)}^\dagger (X_{1,(x,y)}^\dagger)^2 X_{1,(x+1,y)} X_{1,(x-1,y)}, \\ P_{(x,y+1/2)} &:= Z_{1,(x,y+1)} Z_{1,(x,y)}^\dagger (Z_{2,(x,y+1/2)}^\dagger)^2 Z_{2,(x-1,y+1/2)} Z_{2,(x+1,y+1/2)}. \end{aligned} \quad (4)$$

These terms are portrayed in Fig. 1(b)(c). We interchangeably call these two terms,  $V_{(x,y)}$  and  $P_{(x,y+1/2)}$ , *vertex* and *plaquette operators*, respectively. It is straightforward to check that each term in (4) commute, forming the stabilizer group. Hamiltonian is defined by

$$H = - \sum_{(x,y)} V_{(x,y)} - \sum_{(x,y+1/2)} P_{(x,y+1/2)} + h.c. \quad (5)$$

This model shares the same feature as the  $\mathbb{Z}_N$  toric code [25]. The ground state is the stabilized state: the ground state  $|\Omega\rangle$  satisfies

$$V_{(x,y)} |\Omega\rangle = P_{(x,y+1/2)} |\Omega\rangle = |\Omega\rangle \quad \forall V_{(x,y)}, P_{(x,y+1/2)}.$$

Also, our model admits two types of fractional excitations when the condition  $V_{(x,y)} = 1$  or  $P_{(x,y+1/2)} = 1$  is violated at a vertex or link. The crucial difference between our model and the toric code is that that each terms in the Hamiltonian involves not only nearest neighboring sites but also next nearest neighboring ones. As a consequence, the fractional excitations are subject to mobility constraint, giving rise to unusual GSD dependence on the system size. We dub

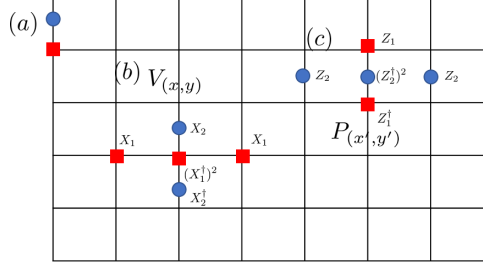


FIG. 1: (a) Two types of  $\mathbb{Z}_N$  clock states, defined on each vertex (red square) and vertical link (blue dot). (b)(c) Two types of terms introduced in (4).

the topological phases with this feature *higher rank topological phases*. Throughout this paper, we consider the model placed on the torus geometry with length in the  $x(y)$  direction being  $n_x(n_y)$ .

### B. Simplest case: $N = 2$

Before discussing the model for generic case of  $N$ , we consider the simplest case by setting  $N = 2$  to make more intuitive understanding of our model (5). The argument presented here will be useful to interpret our result on the entanglement entropy (Sec. IV). In this case, the terms defined in (4) become

$$\begin{aligned} V_{(x,y)} &= X_{2,(x,y+1/2)} X_{2,(x,y-1/2)} X_{1,(x-1,y)} X_{1,(x+1,y)}, \\ P_{(x,y+1/2)} &= Z_{1,(x,y+1)} Z_{1,(x,y)} Z_{2,(x-1,y+1/2)} Z_{2,(x+1,y+1/2)}. \end{aligned} \quad (6)$$

One can regard each term as the plaquette term in a rhombus shape, as portrayed in Fig. 2a. The Hamiltonian (5) with (6) resembles the  $\mathbb{Z}_2$  toric code. However there is a crucial difference between the two: each term (6) involves *next* nearest neighboring Pauli operators in the  $x$ -direction, as opposed to the regular toric code where each term consists of nearest neighboring Pauli operators. Due to this property, one can separate the mutually commuting terms (6) into two groups without considering the boundary:

$$(i) \{V_{(2m,y)}, P_{(2m'-1,y'+1/2)}\}, \quad (ii) \{V_{(2m-1,y)}, P_{(2m',y'+1/2)}\} \quad (m, m' \in \mathbb{Z}). \quad (7)$$

Hence, without thinking the boundary, the model that we describe with  $N = 2$  amounts to be two decoupled  $\mathbb{Z}_2$  toric codes.

Now we impose boundary condition on the lattice. We impose periodic boundary condition in both of  $x$ - and  $y$ -direction, assuming the length of the lattice in the  $x$ -direction is even. In this case,

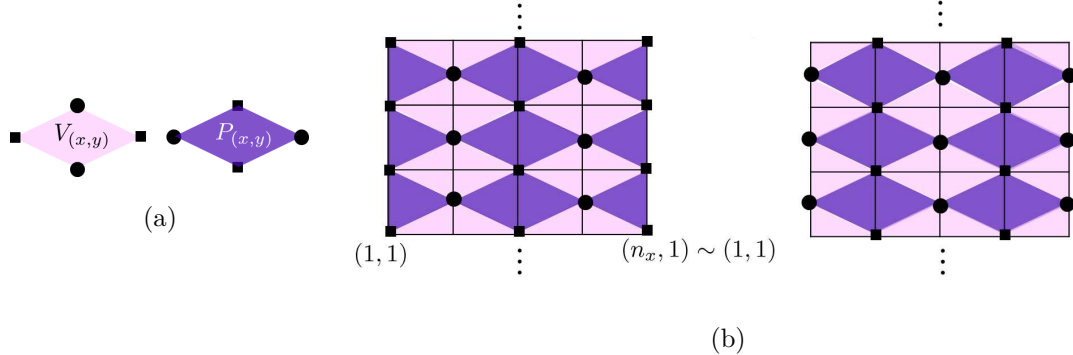


FIG. 2: (a) Two terms defined in (6) constituting the Hamiltonian in the case of  $N = 2$ . (b) Configurations of stabilizers corresponding to (7) in the case of  $n_x$  even. In this case, the model is decomposed into two  $\mathbb{Z}_2$  toric codes. The periodic boundary condition is imposed in the  $x$ -direction so that left and right edge are identified. The left [right] geometry corresponds to configuration of the vertex and plaquette terms which belong to (i)[(ii)] defined in (7). Such decomposition is not possible in the case of  $n_x$  being odd. We set the coordinate of the vertex at the bottom left to be  $(1, 1)$ .

the Hamiltonian (5) consists of two decoupled  $\mathbb{Z}_2$  toric codes on the torus. Such decomposition is portrayed in Fig. 2b. In each  $\mathbb{Z}_2$  toric code, there are two types of  $\mathbb{Z}_2$  excitations, electric and magnetic charge. The non-local string of these charges yields logical operators, giving rise to fourfold GSD on the torus [25, 32]. Therefore, GSD of our model is found to be  $4^2 = 16$ . On the contrary, the situation is drastically different when the length of the lattice in the  $x$ -direction is odd, instead of even. In this case, one cannot separate the terms (6) into two groups, thus the decomposition (7) is no longer true. Indeed, the terms belonging to (i) in (7) are “connected” with the ones belonging to (ii). For instance, the terms  $V_{(n_x-1,y)}$  which belong to (i) in (7) and  $V_{n_x+1,y} = V_{1,y}$  belonging to (ii) (equality follows from the periodic boundary condition) are located to adjacent each other. Therefore, the model is equivalent to one  $\mathbb{Z}_2$  toric code on torus, giving  $GSD = 4$ .

To summarize the argument presented in this subsection, in the simplest case by setting  $N = 2$ , we learn that our model is identified as the  $\mathbb{Z}_2$  toric code where each plaquette term is in a rhombus shape and that its GSD on torus, drastically changes depending on the length of the lattice in the

$x$ -direction, i.e.,

$$\text{GSD} = \begin{cases} 16 & (n_x \text{ even}) \\ 4 & (n_x \text{ odd}). \end{cases} \quad (8)$$

Such behavior can be understood by the fractional excitations with mobility constraint, analogously to the fracton topological phases. (See [30] for more details.) In the next subsection, we turn to the generic cases of  $N$  and discuss its topological properties.

### C. Logical operators and Ground state degeneracy

In this subsection, we discuss our model in the generic cases of  $N$ . As opposed to the case with  $N = 2$ , identifying the GSD and the logical operators is not so immediate in the generic case of  $N$ . Thus, we employ an alternative approach to accomplish this task. We adopt an algebraic tool of the graph theory, which will play a pivotal role in the subsequent discussion on the entanglement entropy. As we mentioned below (5), each term of the Hamiltonian involves the clock states in the next nearest neighboring as well as the nearest neighbor ones. Such feature can be succinctly described by the *Laplacian matrix* (*Laplacian*, in short), the graph theoretical analogue of the second order derivatives [33].

To this end, at each  $y$  on the lattice, we define the Laplacian  $L$  as the  $n_x \times n_x$  matrix indexed by vertices  $(x, y)$  ( $1 \leq x \leq n_x$ )  $\exists y$  running in the  $x$ -direction, which has the following form:

$$L = \begin{pmatrix} 2 & -1 & & & -1 \\ -1 & 2 & -1 & & \\ & -1 & 2 & \ddots & \\ & & \ddots & \ddots & -1 \\ -1 & & & -1 & 2 \end{pmatrix} \quad (9)$$

Equivalently,

$$(L)_{x,x'} = \begin{cases} 2 & (x = x') \\ -1 & (x = x' \pm 1) \\ 0 & (\text{else}), \end{cases} \quad (10)$$

where we have conventionally defined  $x = n_x + 1 = 1$  due to the periodic boundary condition. The term  $V_{(x,y)}$  at given  $y$ , constituting the Hamiltonian (4) now can be rewritten in terms of the

matrix element of the Laplacian (10) via

$$V_{(x,y)} = X_{2,(x,y+1/2)} X_{2,(x,y-1/2)}^\dagger X_{1,(x,y)}^{-(L)_{x,x}} X_{1,(x+1,y)}^{-(L)_{x+1,x}} X_{1,(x-1,y)}^{-(L)_{x-1,x}}, \quad (11)$$

where we conventionally set  $X_{1,(x,y)}^{-1} = X_{1,(x,y)}^\dagger$ . Likewise, each term of  $P_{(x,y+1/2)}$  can be rewritten in the similar manner as

$$P_{(x,y)} = Z_{1,(x,y+1)} Z_{1,(x,y)}^\dagger Z_{2,(x,y+1/2)}^{-(L)_{x,x}} Z_{2,(x-1,y+1/2)}^{-(L)_{x-1,x}} Z_{2,(x+1,y+1/2)}^{-(L)_{x+1,x}}. \quad (12)$$

With this preparation, we now turn to counting the GSD on the torus geometry. The GSD is obtained by the number of total clock states divided by the number of independent stabilizers. The number of the clock states is found to be  $N^{2n_x n_y}$ . Also, the total number of the stabilizers (4) is given by  $N^{2n_x n_y}$ . However, we have over-counted the number of stabilizers; we need to take into account the constraint on the stabilizers as multiplication of some of stabilizers becomes identity. To find such constraint, we resort to the formalism of the Laplacian (9). At given  $y$ , introducing  $n_x$  dimensional vector  $\mathbf{r} := (r_1, \dots, r_{n_x})^T \in \mathbb{Z}_N^{n_x}$ , we consider following product of the vertex operators in the  $x$ -direction

$$\prod_{x=1}^{n_x} V_{(x,y)}^{r_x}.$$

Referring to (11), we transform it by using the Laplacian  $L$  as

$$\prod_{x=1}^{n_x} V_{(x,y)}^{r_x} = \left[ \prod_{x=1}^{n_x} \{X_{2,(x,y+1/2)}^\dagger X_{2,(x,y-1/2)}\}^{r_x} \right] \times \prod_{x=1}^{n_x} X_{1,(x,y)}^{s_x} \quad (s_x \in \mathbb{Z}_N) \quad (13)$$

with

$$\mathbf{s} := (s_1, \dots, s_{n_x})^T = -L\mathbf{r}. \quad (14)$$

Suppose  $\mathbf{s} = \mathbf{0} \pmod{N}$ . Then, multiplying the operators (13) along the  $y$ -direction gives (see also Fig. 3a)

$$\prod_{y=1}^{n_y} \left( \prod_{x=1}^{n_x} V_{(x,y)}^{r_x} \right) = \prod_{y=1}^{n_y} \left[ \prod_{x=1}^{n_x} \{X_{2,(x,y+1/2)}^\dagger X_{2,(x,y-1/2)}\}^{r_x} \right] = I, \quad (15)$$

where the last equation holds due to the periodic boundary condition. Therefore, to find constraints of the stabilizers, we need to evaluate the solution of

$$L\mathbf{r} = \mathbf{0} \pmod{N}, \quad (16)$$

i.e., the kernel of the Laplacian.

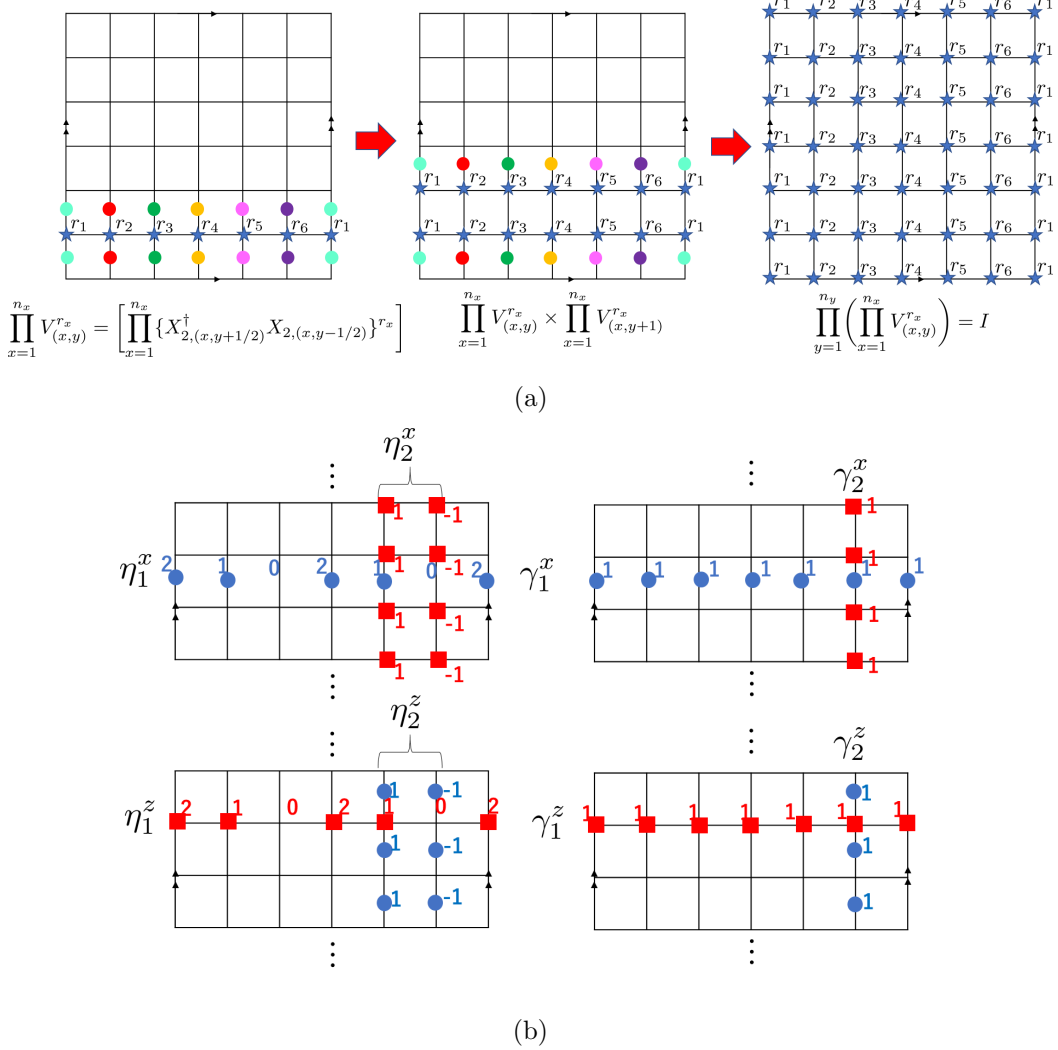


FIG. 3: (a) [Left] Configuration of the product of the operators  $V_{(x,y)}$  (blue stars) given in (13),  $\prod_{x=1}^{n_x} V_{(x,y)}^{r_x}$  with  $s = 0$ . Since  $s = 0$ , it does not have  $X_1$  operators in the horizontal direction, leaving  $X_2$ 's in the vertical links (dots). [Middle] If we multiply the product (13) with the adjacent one in the  $y$ -direction, some of  $X_2$ 's are cancelled out. [Right] Iterating the similar procedure, one obtains the product of (13) all along in the  $y$ -direction,  $\prod_{y=1}^{n_y} \left( \prod_{x=1}^{n_x} V_{(x,y)}^{r_x} \right)$ , which is identity due to the periodic boundary condition. (b) [Top] Configurations of the logical operators constructed by non-contractible loops of  $X_1$  or  $X_2$  operators defined in (23) in the case of  $N = 3$  and  $n_x = 6$ . [Bottom] Logical operators defined in (25) with  $N = 3$  and  $n_x = 6$ . The periodic boundary condition is imposed so that the left and right edge are identified.

To proceed, we transform the Laplacian into the diagonal form, known as the *Smith normal form*. Introducing invertible integer matrices  $P$  and  $Q$ , one can transform the Laplacian (9) as

$$PLQ = D, \quad D = \text{diag}(\underbrace{1, \dots, 1}_{n_x-2}, n_x, 0), \quad (17)$$

With this transformation, one can rewrite (16) as

$$\begin{aligned} (16) \Leftrightarrow P^{-1}DQ^{-1}\mathbf{r} &= \mathbf{0} \pmod{N} \\ \Leftrightarrow D\tilde{\mathbf{r}} &= \mathbf{0} \pmod{N}. \end{aligned} \quad (18)$$

When moving from the second to the third equation, we have used the fact that  $P$  is the integer matrix. Also, we have defined  $\tilde{\mathbf{r}} := Q^{-1}\mathbf{r}$ . From (17) (18), it follows that

$$\tilde{r}_i = 0 \quad (1 \leq i \leq n_x - 2), \quad n_x \tilde{r}_{n_x-1} = 0 \pmod{N}. \quad (19)$$

The last entry of the vector  $\tilde{\mathbf{r}}$ ,  $\tilde{r}_{n_x}$  takes  $N$  distinct values since the last diagonal element of the matrix  $D$  is zero [(17)]. Taking this fact as well as (19) into account, we have

$$\tilde{\mathbf{r}} = (\underbrace{0, \dots, 0}_{n_x-2}, N'\alpha_1, \alpha_2)^T, \quad N' := \frac{N}{\gcd(N, n_x)}, \quad (\alpha_1 \in \mathbb{Z}_{\gcd(N, n_x)}, \alpha_2 \in \mathbb{Z}_N). \quad (20)$$

Here,  $\gcd$  stands for the greatest common divisor. By evaluating the form of the matrix  $Q$  [30], one finds

$$\mathbf{r} = Q\tilde{\mathbf{r}} = N'\alpha_1 \begin{pmatrix} n_x-1 \\ n_x-2 \\ \vdots \\ 1 \\ 0 \end{pmatrix} + \alpha_2 \begin{pmatrix} 1 \\ 1 \\ \vdots \\ 1 \\ 1 \end{pmatrix} \pmod{N}. \quad (21)$$

Therefore, there are  $\gcd(N, n_x) \times N$  constraints on the stabilizers  $V_{(x,y)}$ .

One can analogously discuss the number of the constraints on the stabilizers  $P_{(x,y+1/2)}$ , yielding that there are  $\gcd(N, n_x) \times N$  constraints. Overall, there are  $[\gcd(N, n_x) \times N]^2$  constraints on the stabilizers, hence, the GSD is given by

$$GSD = \frac{N^{2n_x n_y}}{N^{2n_x n_y}/[\gcd(N, n_x) \times N]^2} = [\gcd(N, n_x) \times N]^2. \quad (22)$$

It is emphasized that our model exhibits unusual GSD dependence on the system size which was not seen in fracton topological phases which exhibit the sub-extensive GSD.

One can make use of the formalism of the Laplacian to identify the form of the logical operators. By evaluating the kernel and cokernel of the Laplacian (see [30] for derivation), one can introduce logical operators consisting of non-contractible loop of  $X_1$  or  $X_2$  operators as

$$\begin{aligned}\eta_1^x &= \prod_{x=1}^{n_x} X_{2,(x,y+1/2)}^{p_x}, \quad \gamma_1^x = \prod_{x=1}^{n_x} X_{2,(x,y+1/2)}^{q_x}, \\ \eta_2^x &= \left( \prod_{y=1}^{n_y} X_{1,(n_x-1,y+1/2)} \right) \times \left( \prod_{y=1}^{n_y} X_{1,(n_x,y+1/2)}^\dagger \right), \quad \gamma_2^x = \prod_{y=1}^{n_y} X_{1,(n_x,y+1/2)}\end{aligned}\quad (23)$$

with

$$\mathbf{p} = (p_1, p_2, \dots, p_{n_x})^T = N' \alpha_1 \begin{pmatrix} n_x - 1 \\ n_x - 2 \\ \vdots \\ 1 \\ 0 \end{pmatrix}, \quad \mathbf{q} = (q_1, q_2, \dots, q_{n_x})^T = \alpha_2 \begin{pmatrix} 1 \\ 1 \\ \vdots \\ 1 \\ 1 \end{pmatrix} \quad \text{mod } N \quad (24)$$

We portray them in Fig. 3b in the case of  $N = 3$  and  $n_x = 6$ . These operators are represented as  $\eta_m^x, \gamma_m^x$  ( $m = 1, 2$ ), where two types of the loop are labeled by  $\eta$  and  $\gamma$ , whereas the index  $m$  denotes the direction of the loops ( $x$  or  $y$ ). In addition to the logical operators,  $\gamma_1^x, \gamma_2^x$  that one can find in the toric code, there are new form of the logical operators in our model,  $\eta_1^x, \eta_2^x$ . In the horizontal direction,  $\eta_1^x$  is formed by the inhomogeneous string of  $X_2$ 's whereas in the vertical direction, the model admits the “dipole of the loops”, i.e., a pair of the non-contractible loops of  $X_1$ 's in the vertical direction with opposite sign located adjacent to each other, giving  $\eta_2^x$ . The logical operators  $\eta_1^x$  and  $\gamma_1^x$  are topological in that they can be deformed upward or downward in the  $y$ -direction. Also, logical operators  $\eta_2^x$  and  $\gamma_2^x$  are deformable in the  $x$ -direction.

Analogously to (23), logical operators involving  $Z_1$  or  $Z_2$  operators are defined by (Fig. 3b)

$$\begin{aligned}\eta_1^z &= \prod_{x=1}^{n_x} Z_{1,(x,y)}^{p_x}, \quad \gamma_1^z = \prod_{x=1}^{n_x} Z_{1,(x,y)}^{q_x}, \\ \eta_2^z &= \left( \prod_{y=1}^{n_y} Z_{2,(n_x-1,y)} \right) \times \left( \prod_{y=1}^{n_y} Z_{2,(n_x,y)}^\dagger \right), \quad \gamma_2^z = \prod_{y=1}^{n_y} Z_{2,(n_x,y)}\end{aligned}\quad (25)$$

where the integers  $p_x$  and  $q_x$  are determined by (24). It is straightforward to check that

$$\begin{aligned}\eta_1^x \eta_2^z &= \omega^{N'} \eta_2^z \eta_1^x, \quad \gamma_1^x \gamma_2^z = \omega \gamma_2^z \gamma_1^x, \quad \eta_2^x \eta_1^z = \omega^{N'} \eta_1^z \eta_2^x, \quad \gamma_2^x \gamma_1^z = \omega \gamma_1^z \gamma_2^x \\ (\eta_1^x)^{\gcd(N,n_x)} &= (\eta_2^x)^{\gcd(N,n_x)} = (\eta_1^z)^{\gcd(N,n_x)} = (\eta_2^z)^{\gcd(N,n_x)} = I, \\ (\gamma_1^x)^N &= (\gamma_2^x)^N = (\gamma_1^z)^N = (\gamma_2^z)^N = I\end{aligned}\quad (26)$$

with commutation relation between other combinations of the logical operators being trivial. Logical operators with the commutation relation (26) yields the GSD  $[\gcd(N, n_x) \times N]^2$ .

Ground states with such GSD can be constructed by the logical operators. Labeling stabilizers involving  $X_1$  or  $X_2$  operators that are obtained by the product of vertex operators  $V_{(x,y)}$  as

$$G = \{g | g \in \prod_{x,y} V_{(x,y)}^{a_{x,y}}, a_{x,y} \in \mathbb{Z}_N\},$$

we define the following ground state

$$|\psi\rangle := \frac{1}{\sqrt{|G|}} \sum_{g \in G} g |0\rangle \quad (27)$$

where  $|0\rangle$  is the trivial state in the diagonal basis of with the  $Z_1$  and  $Z_2$  operators, satisfying  $Z_{1,(x,y)} |0\rangle = Z_{2,(x,y+1/2)} |0\rangle = |0\rangle$  (the generalization of the “spin-up state” to the clock state). Also,  $|G|$  denotes the total number of the stabilizers  $G$ . One can verify that this state is the stabilized state. The  $[\gcd(N, n_x) \times N]^2$  ground states are labeled by

$$|\xi_{ab,cd}\rangle := (\eta_1^x)^a (\gamma_1^x)^b (\eta_2^x)^c (\gamma_2^x)^d |\psi\rangle \quad (0 \leq a, c \leq \gcd(N, n_x) - 1, 0 \leq b, d \leq N - 1). \quad (28)$$

It is known that the number of distinct fractional excitations in a topological phase on torus geometry is identical to GSD [34]. Moreover, in our model, all of the fractional excitations are Abelian, implying that quantum dimension  $d_a$  of any excitation is one. Taking these into account, one can evaluate the total quantum dimension as

$$\sqrt{\sum_a d_a^2} = N \times \gcd(N, n_x), \quad (29)$$

where we have used the fact that there are  $[N \times \gcd(N, n_x)]^2$  distinct fractional excitations, all of which carry quantum dimension one.

In the next section, we calculate the entanglement entropy of our model with respect to the ground states. In particular, we investigate whether the total quantum dimension (29) enters in the form of the entanglement entropy in the disk geometry.

### III. ENTANGLEMENT ENTROPY

Now we come to the main part of this paper. In this section, we study entanglement entropy of our model defined in the previous section. Our calculations rely on the formulation of the entanglement entropy in the stabilizer codes, invented in [31].

## A. Review of the bipartite entanglement in lattice spin systems

Before we systematically discuss the entanglement entropy of the higher rank topological phases, let's review the formalism of the bipartite entanglement in lattice spin systems proposed in [31]. Readers familiar with this formalism may skip this subsection.

### 1. Reduced density matrix

For a qubit system, the Hilbert space is  $\mathcal{H} = \otimes_j \mathcal{H}_j$ , where  $\mathcal{H}_j = \text{span}\{|0\rangle_j, |1\rangle_j, \dots, |N-1\rangle_j\}$  in the  $\sigma_j^z$  basis, where  $\sigma_j^z$  is generalized Pauli matrix in the  $N$ -clock model. We define a reference state  $|0\rangle := \otimes_j |0\rangle_j$ , namely, all-spin-up state. We define  $E := \otimes_j \{1, \sigma_j^x, \dots, (\sigma_j^x)^{N-1}\}$  to be the Abelian group that rotates spins in an onsite manner. Any state in the Hilbert space can be written as  $g|0\rangle$  for some  $g \in E$  with  $g^N = 1$ . A generic state can be written as

$$|\psi\rangle = \sum_{g \in G \subset E} a_g g|0\rangle, \quad \sum_g |a_g|^2 = 1. \quad (30)$$

Here  $G$  is a subgroup of  $E$  and  $a_g$  is the wavefunction of  $|\psi\rangle$  in the computational basis, namely,  $a_g = \langle 0|g|\psi\rangle$ . Given the state  $|\psi\rangle$ , we can define the corresponding density matrix as

$$\rho_\psi := |\psi\rangle\langle\psi| = \sum_{g,g'} a_g \bar{a}_{g'} g|0\rangle\langle 0|g'^\dagger = \sum_{g,g'} a_g \bar{a}_{gg'} g|0\rangle\langle 0|(gg')^\dagger, \quad (31)$$

where in the last equality we redefined  $g' \rightarrow gg'$ . Once a bipartition of the lattice into subsystem A and its complement B, any element  $g$  can be unambiguously decomposed into the product form  $g = g_A \otimes g_B$ , where  $g_{A/B}$  only acts nontrivially on subsystems A/B, respectively. With the decomposition of the reference state  $|0\rangle = |0\rangle_A \otimes |0\rangle_B$ , we obtain the reduced density matrix of subsystem A by tracing over subsystem B as

$$\begin{aligned} \rho_A &= \sum_n {}_B\langle n|\rho|n\rangle_B = \sum_n \sum_{g,g'} a_g \bar{a}_{gg'} g_A |0\rangle_{AA} \langle 0|(g_A g'_A)^\dagger \cdot {}_B\langle n|g_B|0\rangle_B {}_B\langle 0|(g_B g'_B)^\dagger |n\rangle_B \\ &= \sum_{g,g'} a_g \bar{a}_{gg'} g_A |0\rangle_{AA} \langle 0|(g_A g'_A)^\dagger \cdot {}_B\langle 0|g'_B|0\rangle_B, \end{aligned} \quad (32)$$

where we used the completeness relation  $\sum_n |0\rangle_B \langle 0| = I$ . It is easy to see that nonzero contributions only come from  $g'_B = I_B$ . Define

$$G_A := \{g \in G | g = g_A \otimes I_B\}, \quad G_B := \{g \in G | g = I_A \otimes g_B\}. \quad (33)$$

Then  $g'_B = I_B$  implies  $g' \in G_A$ . The reduced density matrix is rewritten as

$$\rho_A = \sum_{g \in G, g' \in G_A} a_g \bar{a}_{gg'} g_A |0\rangle_{AA} \langle 0|(g_A g'_A)^\dagger. \quad (34)$$

The equivalences between the following statements are proven [31] : 1).  $\rho_A$  is diagonal, 2).  $G_A = \{1\}$ , 3).  $\#g = g_A \cdot g_B$  with both  $g_A \in G_A, g_B \in G_B$  nontrivial for  $g \in G$ .

## 2. Entanglement entropy of a subsystem

We will study the entanglement entropy of subsystem A:

$$S_A = -\text{tr } \rho_A \log \rho_A. \quad (35)$$

Without loss of generality, we can assume the total density matrix  $\rho$  is a pure state. Let  $S$  be the stabilizer group, which contains mutually commuting operators formed from  $G$  that are called *stabilizers*. The codeword space is defined as  $\mathcal{L} = \{|\psi\rangle \in \mathcal{H} \mid U|\psi\rangle = |\psi\rangle, \forall U \in S\}$ . Let us take  $|\psi\rangle = \frac{1}{\sqrt{|G|}} \sum_{g \in G} g|0\rangle$  for the moment. We will study the generic ground states in the Appendix B. Apparently,  $|\psi\rangle \in \mathcal{L}$  as  $g|\psi\rangle = |\psi\rangle, \forall g \in G$ . From (34), we have

$$\rho_A = \frac{1}{|G|} \sum_{g \in G, g' \in G_A} g_A|0\rangle_{AA}\langle 0|(g_A g'_A)^\dagger. \quad (36)$$

Let  $G/G_B$  and  $G_{AB} := G/(G_A \cdot G_B)$  be quotients that contain elements that act freely on  $A$  and  $A \cup B$ , respectively. It is shown that for the ground state (36), the entanglement entropy is described by [31]

$$S_A = \log |G_{AB}|. \quad (37)$$

The details are given in Appendix A. The entanglement entropy of the subsystem  $A$  is given by

$$S_A = \log |G| - \log |G_A| - \log |G_B|, \quad (38)$$

where  $|G|$  denotes the total number of independent stabilizers containing  $X_1$  and  $X_2$ , whereas  $|G_A|$  ( $|G_B|$ ) represents the number of stabilizers containing  $X_1$  and  $X_2$  that have support on  $A$  ( $B$ ).

In the following subsections, we study the entanglement entropy of various geometries based on the formula (38).

## B. Single-row/column geometry

After reviewing formulation of the entanglement entropy, we calculate it in various geometries of subsystems in our model. We evaluate the entanglement entropy with respect to the ground

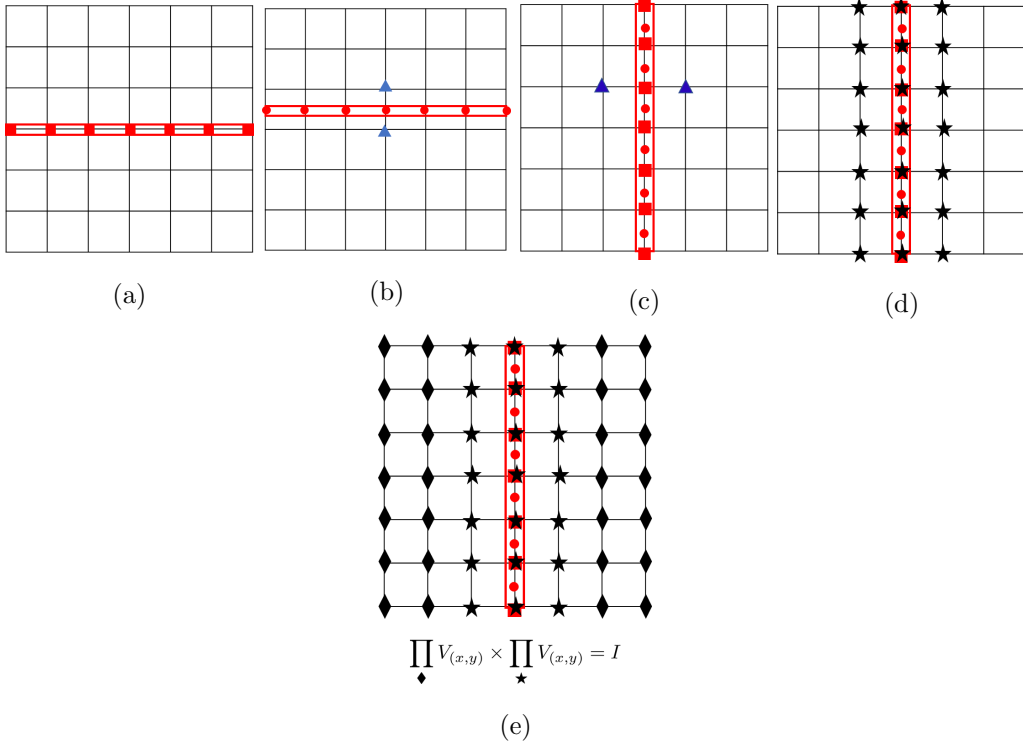


FIG. 4: (a) The subsystem  $A$  is a single row on the horizontal sites (clock states inside the red frame). (b) The subsystem  $A$  is a single row on the vertical links (red dots inside the red frame). The blue triangles represent one of the  $n_x$  constraints along the horizontal direction. (c) The subsystem  $A$  is a single column (red dots and squares inside the frame). The blue triangles represent one of the  $n_y$  constraints along the vertical sites. (d) Multiplication of the vertex operators (represented by black stars) that act within  $B$ . (e) Such product of the stabilizers is redundant due to the constraint that product of all of the vertex operators becomes identity (46).

state  $|\xi_{00,00}\rangle$  given in (28). One could study the entanglement entropy for more generic ground state  $|\zeta\rangle$  which is superposition of  $|\xi_{ab,cd}\rangle$ , defined by

$$|\zeta\rangle = \sum_{a,c=0}^{\gcd(N,n_x)-1} \sum_{b,d=0}^{N-1} \alpha_{ab,cd} |\xi_{ab,cd}\rangle \quad \left( \sum_{abcd} |\alpha_{ab,cd}|^2 = 1, \alpha_{ab,cd} \in U(1) \right). \quad (39)$$

In this case, depending on the geometry of the subsystem  $A$ , there is an additional contribution to (38). While we focus on the entanglement entropy with respect to the ground state  $|\xi_{00,00}\rangle$ , we make a brief comment on the case of the generic ground state (39), deferring the details to Appendix B.

In this subsection, we consider the single-row or-column subsystem geometries which go around

the torus in the  $x$ - or  $y$ -direction, as shown in Fig. 4. When calculating the entanglement entropy based on (38), there is a technical caveat: when evaluating  $|G_A|$  and  $|G_B|$ , we need to take into account product of vertex operators which have support only on  $A$  and  $B$ .

### 1. Single row I

Let's first look at the subsystem A in Fig. (4)(a), we have  $|G| = N^{n_x n_y} / \Gamma$ ,  $|G_A| = 1$ ,  $|G_B| = N^{n_x n_y - n_x}$ , where the factor  $\Gamma$  corresponds to the two independent constraints from (21),  $\Gamma := N \times \gcd(N, n_x)$ . Thus, (38) gives us

$$S_A = n_x \log N - \log N - \log[\gcd(N, n_x)] = n_x \log N - \log \Gamma. \quad (40)$$

For the generic ground state (39), there is an additional constant  $\mu_1$  in (40):

$$S_A = n_x \log N - \log \Gamma + \mu_1, \quad \mu_1 = - \sum_{c,d} \left[ \left( \sum_{a,b} |\alpha_{ab,cd}|^2 \right) \log \left( \sum_{a,b} |\alpha_{ab,cd}|^2 \right) \right] \quad (41)$$

Derivation of (41) is given in Appendix B.

### 2. Single row II

For the subsystem A in Fig. (4)(b), we have

$$|G_A| = 1, |G_B| = (|G|/N^{2n_x}) \cdot N^{n_x} = |G|/N^{n_x},$$

When evaluating  $|G_B|$ , the  $N^{n_x}$  in the first equality comes from the  $n_x$  independent constraints, one of which is labeled by the blue triangles in Fig. (4)(b). Following (38), we have

$$S_A = n_x \log N. \quad (42)$$

In the case of the generic ground state (39), we have an additional contribution to (42):

$$S_A = n_x \log N + \mu_2, \quad \mu_2 = - \sum_{p=0}^{\gcd(N,n_x)-1} \sum_{q=0}^{N-1} \lambda_{p,q} \log \lambda_{p,q} \quad (43)$$

with  $(\nu = e^{2\pi i / \gcd(N, n_x)}, \omega = e^{2\pi i / N})$

$$\lambda_{p,q} = \frac{1}{\Gamma} \sum_{k=0}^{\gcd(N,n_x)-1} \sum_{l=0}^{N-1} \nu^{pk} \omega^{ql} \sigma_{kl}, \quad \sigma_{kl} = \sum_{\substack{a,a',b,b',c,d \\ a-a' \equiv k \pmod{\gcd(N, n_x)} \\ b-b' \equiv l \pmod{N}}} \alpha_{ab,cd} \bar{\alpha}_{a'b',cd}. \quad (44)$$

The derivation of this constant is relegated to Appendix B.

### 3. Single column

Let us turn to subsystem A in Fig. (4)(c). The total number of the independent vertex operators is given by  $|G| = N^{n_x n_y} / \Gamma$ , where we take the constraint discussed in the previous section into consideration (Sec. II C). Next we evaluate  $|G_B|$ . Naively, the number of stabilizers that act within  $B$  is given by

$$N^{n_x n_y - 3n_y} \quad (45)$$

However, this counting is incorrect, as one has to take into account the multiplication of the stabilizers that act trivially on  $A$ . There are two types of such product. The first type is the product of the vertex operators on the both sides of the vertical line. One of such configuration is indicated by the blue triangles in Fig. (4)(c). There are  $N^{n_y}$  such products. Another type is multiplication of the vertex operators which are located inside  $A$  and the ones surrounding  $A$ , as shown in black stars in Fig. (4)(d). Having identified these product of the stabilizers that contribute to  $|G_B|$ , one has to check whether these products are “redundant” to the constraint of the stabilizers that we have already considered.

To be more specific to what we have just said, we look at the second type of the product of the stabilizers that are depicted in Fig. 4(d). We schematically write this product as  $\prod_{\star} V_{(x,y)}$  in accordance with Fig. 4(d). As we discussed in Sec. II C, the multiplication of all of the vertex operators becomes identity, i.e.,

$$\prod_{\blacklozenge} V_{(x,y)} \times \prod_{\star} V_{(x,y)} = I, \quad (46)$$

where  $\prod_{\blacklozenge} V_{(x,y)}$  denotes the product of the vertex operators defined on the complement of  $\star$  [see Fig. 4(e)]. Hence, the product in question,  $\prod_{\star} V_{(x,y)}$  is redundant: it can be generated by the vertex operators belonging to  $B$ . Likewise, regarding the first type of the product, one of which is depicted in Fig. (4)(c), combination of some of them is redundant due to the constraint.

Overall, the multiplication of the vertex operators that act on  $B$  is found to be

$$\frac{N^{n_y} \times N}{[\gcd(N, n_x) \times N]}. \quad (47)$$

Therefore,  $|G_B|$  is obtained by multiplying this number with (45), that is,

$$|G_B| = N^{n_x n_y - 3n_y} \times \frac{N^{n_y} \times N}{[\gcd(N, n_x) \times N]}. \quad (48)$$

There is no stabilizer that act within  $A$ , giving  $|G_A| = 1$ . Referring to (38), the entanglement entropy is given by

$$S_A = 2n_y \log N - \log N. \quad (49)$$

In the case of the generic ground state (39),

$$S_A = 2n_y \log N - \log N + \mu_3, \quad \mu_3 = - \sum_{b=0}^{N-1} \sum_{q=0}^{N-1} \lambda_q^{(b)} \log \lambda_q^{(b)}, \quad (50)$$

where

$$\lambda_q^{(b)} = \frac{1}{N} \sum_{k=0}^{N-1} \omega^{kq} \sigma_k^{(b)}, \quad \sigma_k^{(b)} = \sum_{\substack{a,c,d,d' \\ d-d'=k \pmod{N}}} \alpha_{ab,cd} \bar{\alpha}_{ab,cd'}. \quad (51)$$

The derivation is given in Appendix B.

### C. Disk geometry

Let us calculate entanglement of the contractible disk geometry, as portrayed in Fig. 5a. We assume that width of the disk is more than one. We set the width and height of the disk to be  $l_x (\geq 2)$  and  $l_y$ , respectively. Accordingly, the coordinate of  $\mathbb{Z}_N$  clock states with type 1 (i.e., clock states located at vertices) inside the disk is denoted as  $(x, y)$  ( $x_0 \leq x \leq x_0 + l_x - 1, y_0 \leq y \leq y_0 + l_y - 1$ ) and the ones with type 2 (i.e., clock states at vertical links) inside the disk as  $(x, y + 1/2)$  ( $x_0 \leq x \leq l_x - 1 + x_0, y_0 \leq y \leq y_0 + l_y - 2$ ). See also Fig. 5a.

In this setting, we have  $|G| = N^{n_x n_y} / \Gamma$ ,  $|G_A| = N^{(l_x-2)(l_y-2)}$ . As for  $|G_B|$ , the number of individual stabilizers that have support only on  $B$  is

$$N^{n_x n_y} / N^{l_y(l_x+2)} \quad (52)$$

In addition to this number, we need to take the product of the vertex operators that act within  $B$  into consideration. To find such product, it is useful to resort to the formalism of the Laplacian that we have discussed in Sec. II C. Consider the following product of  $V_{(x,y)}$ 's in the horizontal direction at given  $y$  ( $y_0 \leq y \leq y_0 + l_y - 1$ ) (purple triangles in Fig. 5a)

$$\prod_{x=x_0}^{x_0+l_x-1} V_{(x,y)}^{t_x} \quad (t_x \in \mathbb{Z}_N), \quad (53)$$

which can be rewritten as

$$(53) = \left[ \prod_{x=x_0}^{x_0+l_x-1} \{X_{2,(x,y+1/2)}^\dagger X_{2,(x,y-1/2)}\}^{t_x} \right] \times \prod_{x=1}^{n_x} X_{1,(x,y)}^{u_x} \quad (u_x \in \mathbb{Z}_N). \quad (54)$$

Analogously to the discussion in the previous section, Sec. II C,  $\mathbb{Z}_N$  numbers  $t_x$  and  $u_x$  that appear in (53) (54) are related via Laplacian. Defining  $l_x + 2$ - and  $n_x$ -dimensional vector by  $\mathbf{t} := \underbrace{(t_{x_0-1}, \dots, t_{x_0+l_x})^T}_{l_x+2}$ , and  $\mathbf{u} := \underbrace{(u_1, \dots, u_{n_x})^T}_{n_x}$ , respectively, and referring to (9) (10), we have

$$\mathbf{u} = -\tilde{L}\mathbf{t}. \quad (55)$$

Here,  $\tilde{L}$  represents a sub-matrix of the Laplacian  $L$  (10). It is obtained by decomposing the Laplacian into three matrices as

$$L = \begin{pmatrix} & & \\ L' & \tilde{L} & L'' \\ & & \end{pmatrix}, \quad (56)$$

where  $L'$ ,  $\tilde{L}$ ,  $L''$  is  $n_x \times (x_0 - 2)$ ,  $n_x \times (l_x + 2)$ ,  $n_x \times (n_x - x_0 - l_x)$  sub-matrix, respectively, and concentrating on the middle matrix,  $\tilde{L}$  (see also Fig. 5b).

Suppose the product we consider (54) with (55) has no  $X_1$  operators within the disk  $A$ , that is,

$$\mathbf{u} = (u_1, \dots, u_{x_0-1}, \underbrace{0, \dots, 0}_{l_x}, u_{x_0+l_x}, \dots, u_{n_x})^T. \quad (57)$$

Then, multiplying the product (54) along the  $y$ -direction gives

$$\prod_{y=y_0}^{y_0+l_y-1} \left[ \prod_{x=x_0}^{x_0+l_x-1} V_{(x,y)}^{t_x} \right] \quad (58)$$

which yields the stabilizers that have support only on  $B$  (see Fig. 5c). Therefore, to find the product of stabilizers that acts within  $B$ , we need to evaluate (55) with (57). Such condition can be rewritten as

$$\tilde{L}_{sub}\mathbf{t} = \mathbf{0}, \quad (59)$$

where  $\tilde{L}_{sub}$  denotes the sub-matrix of  $\tilde{L}$ , which is obtained by decomposing the matrix  $\tilde{L}$  into three via

$$\tilde{L} = \begin{pmatrix} & \tilde{L}_1 & \\ & \tilde{L}_{sub} & \\ & \tilde{L}_2 & \end{pmatrix}, \quad (60)$$

where  $\tilde{L}_1$ ,  $\tilde{L}_{sub}$ , and  $\tilde{L}_2$  is the  $(x_0 - 1) \times (l_x + 2)$ ,  $l_x \times (l_x + 2)$ , and  $(n_x - l_x - x_0 + 1) \times (l_x + 2)$  matrix, respectively, and focusing on the middle matrix  $\tilde{L}_{sub}$  (Fig. 5b). From (9) (56) (60), the

explicit form of  $\tilde{L}_{sub}$  is given by

$$\tilde{L}_{sub} = \begin{pmatrix} -1 & 2 & -1 & & & & \\ & -1 & 2 & -1 & & & \\ & & -1 & 2 & \ddots & & \\ & & & \ddots & \ddots & -1 & \\ & & & & & -1 & 2 & -1 \end{pmatrix}. \quad (61)$$

Introducing  $l_x \times l_x$  and  $(l_x + 2) \times (l_x + 2)$  invertible matrices,  $\tilde{P}$  and  $\tilde{Q}$ , whose matrix elements are integers, one can transform the matrix  $\tilde{L}_{sub}$  into the Smith normal form as  $\tilde{P}\tilde{L}_{sub}\tilde{Q} = \tilde{D}$  with

$$\tilde{D} = \begin{pmatrix} 1 & & & & & \\ & 1 & & & & \\ & & 1 & & & \\ & & & \ddots & & \\ & & & & & \\ & & & & & 1 & 0 & 0 \end{pmatrix}. \quad (62)$$

The  $l_x \times (l_x + 2)$  matrix  $\tilde{D}$  contains diagonal entries  $\text{diag}(\underbrace{1, \dots, 1}_{l_x})$  with other entries being zero.

With this form, it follows that

$$\tilde{L}_{sub}\mathbf{t} = \mathbf{0} \Leftrightarrow \tilde{D}\tilde{\mathbf{t}} = \mathbf{0} \pmod{N}, \quad (63)$$

where  $\tilde{\mathbf{t}} := \tilde{Q}^{-1}\mathbf{t}$  and  $\mathbf{0}$  represents  $l_x$ -dimensional zero vector. We rename the entries of the vector  $\tilde{\mathbf{t}}$  as  $\tilde{\mathbf{t}} = (\tilde{t}_1, \dots, \tilde{t}_{l_x+2})^T$ . From the Smith normal form (62) and (63), the first  $l_x$  entries of the vector  $\tilde{\mathbf{t}}$  are subject to

$$\tilde{t}_i = 0 \quad (1 \leq i \leq l_x), \quad (64)$$

whereas there is no constraint on the last two entries  $\tilde{t}_{l_x+1}, \tilde{t}_{l_x+2}$ , giving

$$\tilde{t}_{l_x+1} = \beta_1, \quad \tilde{t}_{l_x+2} = \beta_2 \quad (\beta_1, \beta_2 \in \mathbb{Z}_N). \quad (65)$$

Hence, there are  $N^2$  solutions of (59).

One has to check that such  $N^2$  product of vertex operators which have support only on  $B$  is redundant to the constraint of the stabilizers, analogously to the discussion presented around (46). Thus, the number of product of the stabilizers that act within  $B$  is given by  $\frac{N^2}{\Gamma}$ .

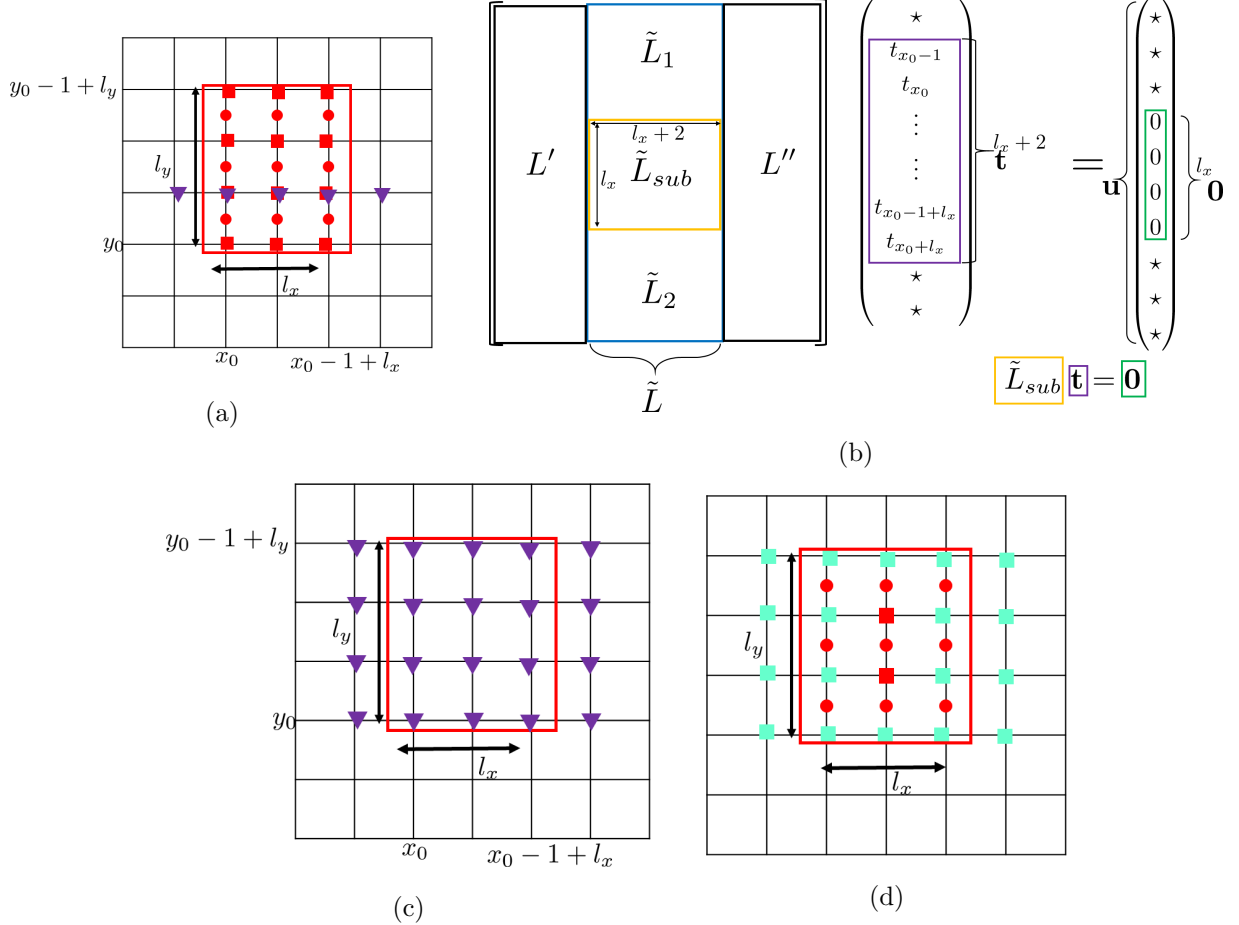


FIG. 5: (a) Disk geometry. The clock states inside the disk are marked by red squares and dots. Purple triangles represent the product given in (53). (b) Decomposition of the Laplacian into sub-matrices, corresponding to (56) (60). We need to find multiplication of the vertex operators corresponding to the vector  $\mathbf{t}$  which does not have  $X_1$  operators inside the disk, yielding the condition (59). (c) Configuration of the product given in (58) (purple triangles). With the condition (57), it exclusively acts on  $B$ . (d) The number of the clock states marked by light-blue squares gives rise to the area-law term, (*Area*), given in (67), which is (*Area*) =  $4l_y + 2(l_x - 2)$  in the present case.

Overall, we obtain  $|G_B|$  by multiplying this number with (52):

$$|G_B| = \frac{N^{n_x n_y}}{N^{l_x(l_y+2)}} \times \frac{N^2}{\Gamma}. \quad (66)$$

From (38), we finally arrive at

$$S_A = (\text{Area}) \log N - 2 \log N. \quad (67)$$

Here,  $(Area)$  is the number of vertex operators that have support on both of  $A$  and its complement,  $B$ , which can be regarded as the number of clock states with type 1 (i.e., clock states located at vertices) surrounding the disk geometry  $A$  (see Fig. 5d). In the present case, it is given by  $(Area) = 4l_y + 2(l_x - 2)$ . One can check that the entanglement entropy of the disk geometry for the generic ground state (39) gives the same answer as (67).

The first term in (67) is nothing but the area law term and the second term, which is the sub-leading term of the entanglement entropy, is of particular importance. It is “topological”; one can confirm that the second term remains the constant when we deform the shape of the disk geometry retaining its topology. Therefore, we have found the same scaling behavior of the entanglement entropy as the one obtained in conventional topologically ordered phases (1). However, there is a crucial deference between the two. In the case of the conventional topologically ordered phases, the topological entanglement entropy  $\gamma$  is related to the total quantum dimension via  $\gamma = \log \sqrt{\sum_a d_a^2}$ , where  $a$  labels the distinct types of fractional excitations. On the contrary, in our case, such a relation does not hold as the number of distinct number of fractional excitations varies depending on the system size [(29)] and the topological entanglement entropy takes a constant number,  $\gamma = -2 \log N$  irrespective to the system size, implying the incapability to associate  $\gamma$  to the total quantum dimension. In the next section, we give a physical interpretation of this result in the simplest setting, i.e.,  $N = 2$ .

	$ \xi_{00,00}\rangle$	generic ground state $ \zeta\rangle$ (39)
single row I [Fig. 4a]	$n_x \log N - \log \Gamma$	$n_x \log N - \log \Gamma + \mu_1$ (41)
single row II [Fig. 4b]	$n_x \log N$	$n_x \log N + \mu_2$ (43) (44)
single column [Fig. 4c]	$2n_y \log N - \log N$	$2n_y \log N - \log N + \mu_3$ (50)(51)
disk geometry [Fig. 5a]	$(Area) \log N - 2 \log N$	$(Area) \log N - 2 \log N$

TABLE I: Summary of the entanglement entropy  $S_A$  of various subsystem geometries with respect to the ground state  $|\xi_{00,00}\rangle$  and the one with the generic ground state (39). Here,  $\Gamma = N \times \text{gcd}(N, n_x)$  and  $(Area)$  represents the number of clock states with type 1 surrounding the disk geometry.

We summarize the results obtained in this section in Table. I

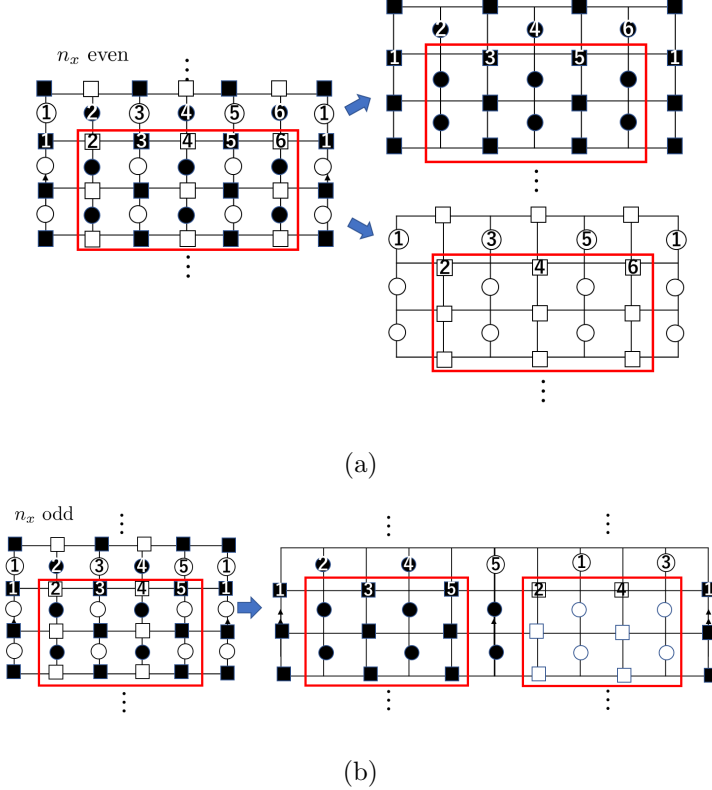


FIG. 6: (a) In the case of  $n_x$  being even. One can decompose the lattice into two. The periodic boundary condition is imposed so that the left and right edge are identified. (b) In the case of  $n_x$  being odd. We double the lattice by going around the torus twice, and omit vertices and links as explained in the main text. The red frame corresponds to the subsystem  $A$  with disk shape considered in the previous section.

#### IV. ALTERNATIVE INTERPRETATION OF THE RESULT IN THE SIMPLEST CASE

In this section, we give an intuitive understanding of the topological entanglement entropy found in the second term of (67) by focusing on the simplest case of  $N$ , i.e.,  $N = 2$ . To this end, discussion presented in Sec. II B is of usefulness.

Recalling the argument in Sec. II B, in the case of  $N = 2$ , depending on whether the length of the lattice in the  $x$ -direction is even or odd, the GSD, accordingly, the total quantum dimension changes whereas the topological entanglement entropy gives  $-2 \log 2$ . Even though we have the topological entanglement entropy  $-2 \log 2$  irrespective to the length of the lattice in the  $x$ -direction being even or odd, its topological origin to have such a number is rather different in these two cases.

As seen from (12), in the case of  $N = 2$  and  $n_x$  being even, the mutually commuting terms

of Hamiltonian get simplified, allowing us to decompose the Hamiltonian into two sectors, each of which describes the  $\mathbb{Z}_2$  toric code. Such decomposition is shown in Fig. 6a where we separate vertices with even number  $x$  coordinate (white squares) and the ones with odd number (black squares) as well as vertical links with odd number  $x$  coordinate (white dots) and the ones with even number (black dots). Correspondingly, the entanglement entropy  $S_A$  is decomposed into two, each of which is the one of the disk geometry in the  $\mathbb{Z}_2$  toric code. Since the topological entanglement entropy of the disk geometry in the  $\mathbb{Z}_2$  toric code is known to be  $-\log 2$  [10, 11], in total, the topological entanglement entropy gives  $2 \times (-\log 2) = -2 \log 2$ .

On the contrary, in the case of  $n_x$  being odd, such decomposition (7) is not valid, thus the Hamiltonian describes one  $\mathbb{Z}_2$  toric code. To see this more clearly, recalling the fact that each commuting term of the Hamiltonian involves next nearest neighboring Pauli operators in the  $x$ -direction, we think of doubling the lattice, obtained by going around the torus in the  $x$ -direction twice and rearranging the vertices and links.

To be more specific to what we have just mentioned, consider a geometry portrayed in Fig. 6b. We double the lattice obtained by traveling around the torus in the  $x$ -direction twice. In the first half of the doubled lattice, we omit the vertices with even number  $x$  coordinate and vertical links with odd number  $x$  coordinate whereas in the latter half, we discard the vertices with odd number  $x$  coordinate and vertical links with even number  $x$  coordinate. Recalling (6), one is convinced that the Hamiltonian describes one  $\mathbb{Z}_2$  toric code on the torus. By this rearrangement, the entanglement entropy  $S_A$  amounts to be the one of two spatially separated disks in the  $\mathbb{Z}_2$  toric code. The topological entanglement entropy is found to be  $-2 \log 2$  – the same value as the case of  $n_x$  even.

## V. BRIEF COMMENTS ON OTHER CASES OF THE HIGHER RANK TOPOLOGICAL PHASES

We have studied entanglement entropy of the higher rank topological phases defined in (5) by making use of formalism of the stabilizers [31] jointly with the one of the Laplacian. One could study entanglement entropy of other higher rank topological phases by resorting to the similar approach.

One example is the model studied recently in [35], which is introduced as follows. At each vertex of the square lattice, we introduce two clock states  $|a\rangle_{(x,y)}|b\rangle_{(x,y)}$ ,  $a, b \in \mathbb{Z}_N$ . Also, define

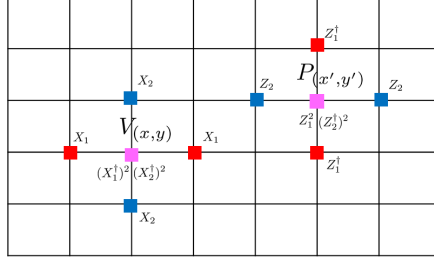


FIG. 7: Two types of terms defined in (69).

operators acting on these states as (recall that  $\omega = e^{2\pi i/N}$ )

$$\begin{aligned} Z_{1,(x,y)} |a\rangle_{(x,y)} |b\rangle_{(x,y)} &= \omega^a |a\rangle_{(x,y)} |b\rangle_{(x,y)}, \quad Z_{2,(x,y)} |a\rangle_{(x,y)} |b\rangle_{(x,y)} = \omega^b |a\rangle_{(x,y)} |b\rangle_{(x,y)} \\ X_{1,(x,y)} |a\rangle_{(x,y)} |b\rangle_{(x,y)} &= |a+1\rangle_{(x,y)} |b\rangle_{(x,y)}, \quad X_{2,(x,y)} |a\rangle_{(x,y)} |b\rangle_{(x,y)} = |a\rangle_{(x,y)} |b+1\rangle_{(x,y)}. \end{aligned} \quad (68)$$

Introducing the following terms by (Fig. 7)

$$\begin{aligned} V_{(x,y)} &:= X_{1,(x+1,y)} X_{1,(x-1,y)} (X_{1,(x,y)}^\dagger)^2 X_{2,(x,y+1)} X_{2,(x,y-1)} (X_{2,(x,y)}^\dagger)^2 \\ P_{(x,y)} &:= Z_{1,(x,y+1)}^\dagger Z_{1,(x,y-1)}^\dagger Z_{1,(x,y)}^2 Z_{2,(x+1,y)} Z_{2,(x-1,y)} (Z_{2,(x,y)}^\dagger)^2, \end{aligned} \quad (69)$$

Hamiltonian reads

$$H_{\mathbb{Z}_N} = - \sum_{x,y} (V_{(x,y)} + P_{(x,y)}). \quad (70)$$

The GSD of the phase on the torus geometry with length of the lattice in the  $x$  and  $y$  direction being  $n_x$  and  $n_y$ , is found to be [35]

$$GSD = [N \times \gcd(N, n_x) \times \gcd(N, n_y) \times \gcd(N, n_x, n_y)]^2. \quad (71)$$

By making use of the similar line of thoughts outlined in Sec. III, one obtains the entanglement entropy of the disk geometry as

$$S_A = (\text{Area}) \log N - 4 \log N. \quad (72)$$

Here,  $\text{Area}$  is the number of vertices surrounding the disk. Compared with the result (67), the absolute value of the topological entanglement entropy is increased. Also, the total quantum dimension of the model is given by  $\sqrt{\sum_a d_a^2} = [N \times \gcd(N, n_x) \times \gcd(N, n_y) \times \gcd(N, n_x, n_y)]$ , thus, analogously to (67), the relation between total quantum dimension and the topological entanglement entropy does not hold.

It would be interesting to study other higher rank topological phases, such as the ones studied in [36–38]. Generically, we make a conjecture that one cannot associate the topological entanglement entropy in the higher rank topological phases with the total quantum dimension of the fractional excitations and also that the absolute value of the topological entanglement entropy becomes larger when the model contains the terms which involves clock states in the longer range. We leave confirmation of this speculation for future studies.

## VI. CONCLUSION

In this work, we study entanglement entropy of unusual topological stabilizer models which host fractional excitations with restricted mobility in a manner akin to fracton topological phases. While the GSD and the total quantum dimension of the fractional excitations drastically changes depending on the system size, topological entanglement entropy  $\gamma$  takes a constant, given by  $\gamma = -2 \log N$ . Due to this result, the well-known relation between the topological entanglement entropy and the total quantum dimension is not valid in the case of the higher rank topological phases. Such a result can be understood by decomposition of the model into two or rearrangement of the lattice in the simplest case  $N = 2$ . Our study may contribute to better understanding of fracton topological phases in view of entanglement entropy (see also [39–41] for recent discussions on this subject)

There are several future research directions regarding the present study. It would be interesting to study the entanglement entropy of our model on more generic lattices beyond typical square one. As we have seen in this work, our model nicely fit in with the graph theory, allowing us to systematically study the physical properties of the models by resorting to the algebraic tools of the graph theory such as the Laplacian. It would be illuminating to see how the scaling behavior of the entanglement entropy of the higher rank topological phases on generic lattices is related to other quantities in terms of the graph theory, such as connectivity.

While we focus on the entanglement entropy in the higher rank topological phases, one would be curious to elucidate behavior of other observable to quantify the quantum entanglement. One candidate would be entanglement negativity [42, 43], an important observable to extract quantum correlation rather than classical one. It would be intriguing to investigate the entanglement negativity of our model to see how different it is compared with the case of the conventional topologically ordered phases [44].

## ACKNOWLEDGEMENT

The author thanks Bo Han and Yuval Oreg for helpful discussion. This work was supported in part by a grant from the Simons Foundation (825876, TDN).

---

- [1] A. Einstein, B. Podolsky, and N. Rosen, *Phys. Rev.* **47**, 777 (1935).
- [2] R. Horodecki, P. Horodecki, M. Horodecki, and K. Horodecki, *Rev. Mod. Phys.* **81**, 865 (2009).
- [3] L. Amico, R. Fazio, A. Osterloh, and V. Vedral, *Rev. Mod. Phys.* **80**, 517 (2008).
- [4] L. Bombelli, R. K. Koul, J. Lee, and R. D. Sorkin, *Phys. Rev. D* **34**, 373 (1986).
- [5] M. Srednicki, *Phys. Rev. Lett.* **71**, 666 (1993).
- [6] D. Gioev and I. Klich, *Phys. Rev. Lett.* **96**, 100503 (2006).
- [7] C. Callan and F. Wilczek, *Physics Letters B* **333**, 55 (1994).
- [8] P. Calabrese and J. Cardy, *Journal of Statistical Mechanics: Theory and Experiment* **2004**, P06002 (2004).
- [9] J. I. Latorre, E. Rico, and G. Vidal, *Quantum Info. Comput.* **4**, 48–92 (2004).
- [10] A. Kitaev and J. Preskill, *Phys. Rev. Lett.* **96**, 110404 (2006).
- [11] M. Levin and X.-G. Wen, *Phys. Rev. Lett.* **96**, 110405 (2006).
- [12] S. Ryu and T. Takayanagi, *Phys. Rev. Lett.* **96**, 181602 (2006).
- [13] V. E. Hubeny, M. Rangamani, and T. Takayanagi, *Journal of High Energy Physics* **2007**, 062 (2007), [arXiv:0705.0016 \[hep-th\]](https://arxiv.org/abs/0705.0016).
- [14] A. Lewkowycz and J. Maldacena, *Journal of High Energy Physics* **2013**, 90 (2013), [arXiv:1304.4926 \[hep-th\]](https://arxiv.org/abs/1304.4926).
- [15] T. Faulkner, A. Lewkowycz, and J. Maldacena, *Journal of High Energy Physics* **2013**, 74 (2013), [arXiv:1307.2892 \[hep-th\]](https://arxiv.org/abs/1307.2892).
- [16] N. Engelhardt and A. C. Wall, *Journal of High Energy Physics* **2015**, 73 (2015), [arXiv:1408.3203 \[hep-th\]](https://arxiv.org/abs/1408.3203).
- [17] A. Almheiri, T. Hartman, J. Maldacena, E. Shaghoulian, and A. Tajdini, *Rev. Mod. Phys.* **93**, 035002 (2021).
- [18] D. C. Tsui, H. L. Stormer, and A. C. Gossard, *Phys. Rev. Lett.* **48**, 1559 (1982).
- [19] R. B. Laughlin, *Phys. Rev. Lett.* **50**, 1395 (1983).
- [20] V. Kalmeyer and R. B. Laughlin, *Phys. Rev. Lett.* **59**, 2095 (1987).
- [21] X. G. Wen, F. Wilczek, and A. Zee, *Phys. Rev. B* **39**, 11413 (1989).
- [22] J. M. Leinaas and J. Myrheim, *Il Nuovo Cimento B (1971-1996)* **37**, 1 (1977).
- [23] F. Wilczek, *Phys. Rev. Lett.* **49**, 957 (1982).
- [24] E. Dennis, A. Kitaev, A. Landahl, and J. Preskill, *Journal of Mathematical Physics* **43**, 4452 (2002).
- [25] A. Kitaev, *Annals of Physics* **303**, 2 (2003).

- [26] M. H. Freedman, M. Larsen, and Z. Wang, Communications in Mathematical Physics **227**, 605 (2002).
- [27] C. Chamon, *Phys. Rev. Lett.* **94**, 040402 (2005).
- [28] J. Haah, *Phys. Rev. A* **83**, 042330 (2011).
- [29] S. Vijay, J. Haah, and L. Fu, *Phys. Rev. B* **94**, 235157 (2016).
- [30] H. Ebisu and B. Han, arXiv preprint arXiv:2209.07987.
- [31] A. Hamma, R. Ionicioiu, and P. Zanardi, *Phys. Rev. A* **71**, 022315 (2005).
- [32] A. G. Fowler, M. Mariantoni, J. M. Martinis, and A. N. Cleland, *Phys. Rev. A* **86**, 032324 (2012).
- [33] F. R. Chung and F. C. Graham, *Spectral graph theory*, Vol. 92 (American Mathematical Soc., 1997).
- [34] S. Elitzur, G. W. Moore, A. Schwimmer, and N. Seiberg, *Nucl. Phys. B* **326**, 108 (1989).
- [35] H. Ebisu, arXiv preprint arXiv:2302.03747 (2023).
- [36] D. Bulmash and M. Barkeshli, *Phys. Rev. B* **97**, 235112 (2018).
- [37] S. D. Pace and X.-G. Wen, *Phys. Rev. B* **106**, 045145 (2022).
- [38] P. Gorantla, H. T. Lam, N. Seiberg, and S.-H. Shao, arXiv preprint arXiv:2210.03727 (2022).
- [39] H. He, Y. Zheng, B. A. Bernevig, and N. Regnault, *Phys. Rev. B* **97**, 125102 (2018).
- [40] A. T. Schmitz, H. Ma, R. M. Nandkishore, and S. A. Parameswaran, *Phys. Rev. B* **97**, 134426 (2018).
- [41] B. Shi and Y.-M. Lu, *Phys. Rev. B* **97**, 144106 (2018).
- [42] J. Eisert and M. B. Plenio, *Journal of Modern Optics* **46**, 145 (1999).
- [43] G. Vidal and R. F. Werner, *Phys. Rev. A* **65**, 032314 (2002).
- [44] Y. A. Lee and G. Vidal, *Phys. Rev. A* **88**, 042318 (2013).

### Appendix A: Proof of Eq. (37)

Given  $g, g' \in G$ , we have  $g'_A = g_A \Leftrightarrow g' = hg, h \in G_B$ . Then (36) is reduced to

$$\rho_A = \frac{|G_B|}{|G|} \sum_{g \in G/G_B, g' \in G_A} g_A |0\rangle_{AA} \langle 0| (g_A g'_A)^\dagger. \quad (\text{A1})$$

We have

$$\begin{aligned} \rho_A^2 &= \left( \frac{|G_B|}{|G|} \right)^2 \sum_{g, \tilde{g} \in G/G_B, g', \tilde{g}' \in G_A} g_A |0\rangle_{AA} \langle 0| (g_A \tilde{g}_A)^\dagger g'_A |0\rangle_{AA} \langle 0| (g'_A \tilde{g}'_A)^\dagger \\ &= \left( \frac{|G_B|}{|G|} \right)^2 \sum_{g \in G/G_B, \tilde{g}, \tilde{g}' \in G_A} g_A |0\rangle_{AA} \langle 0| (g_A \tilde{g}_A \tilde{g}'_A)^\dagger \\ &= \left( \frac{|G_B|}{|G|} \right)^2 |G_A| \sum_{g \in G/G_B, \tilde{g} \in G_A} g_A |0\rangle_{AA} \langle 0| (g_A \tilde{g}_A)^\dagger \\ &= \frac{|G_B|}{|G|} |G_A| \rho_A, \end{aligned} \quad (\text{A2})$$

from which one finds

$$\rho_A^n = \left( \frac{|G_A| \cdot |G_B|}{|G|} \right)^{(n-1)} \rho_A. \quad (\text{A3})$$

The entanglement entropy is obtained as

$$S_A = \lim_{n \rightarrow 1} \frac{1}{1-n} \log \text{tr} \rho_A^n = \log \frac{|G|}{|G_A| \cdot |G_B|}. \quad (\text{A4})$$

## Appendix B: Entanglement entropy with respect to the generic ground state

In this section, we give a derivation of the entanglement entropy of three subsystems discussed in Sec. III B in the case of the generic ground state (39). The density matrix  $\rho_A^\zeta$  of a subsystem  $A$  in our model with respect to the generic ground state (39) reads

$$\rho_A^\zeta = \text{Tr}_B |\zeta\rangle \langle \zeta|, \quad (\text{B1})$$

where  $|\zeta\rangle$  is given by (39). From (28), it is explicitly written as

$$\rho_A^\zeta = \sum_{\substack{a,b,c,d \\ a',b',c',d'}} \alpha_{ab,cd} \bar{\alpha}_{a'b',c'd'} \text{Tr}_B [(\eta_1^x)^a (\gamma_1^x)^b (\eta_2^x)^c (\gamma_2^x)^d \rho_0 (\eta_1^x)^{a'} (\gamma_1^x)^{b'} (\eta_2^x)^{c'} (\gamma_2^x)^{d'}] \quad (\text{B2})$$

with  $\rho_0 = |\zeta_{00}\rangle \langle \zeta_{00}|$ . Below we look at the three cases corresponding to Fig. 4a,b,c.

### 1. Single row I

In Fig. (4)(a), recalling the form of the logical operators (23) (see also Fig. 3b), the logical operator  $\eta_1^x$  and  $\gamma_1^x$  act within subsystem B, hence the term  $\text{Tr}_B[\dots]$  in (B2) is transformed as

$$\frac{1}{|G|} \sum_{g,g' \in G} (\eta_{2A}^x)^c (\gamma_{2A}^x)^d g_A |0\rangle_{AA} \langle 0| (g_A g_A')^\dagger (\eta_{2A}^{x\dagger})^{c'} (\gamma_{2A}^{x\dagger})^{d'} \cdot_B \langle 0| g_B'^\dagger (\eta_1^x)^{a-a'} (\gamma_1^x)^{b-b'} (\eta_{2B}^x)^{c-c'} (\gamma_{2B}^x)^{d-d'} |0\rangle_B \quad (\text{B3})$$

where rewrite the logical operator by the product form  $\eta_2^x = \eta_{2A}^x \otimes \eta_{2B}^x$ , and similarly for  $\gamma_2^x$ . From the inner product of the state  $|0\rangle_B$  in (B3), one finds that

$$g'_B = I_B, \quad a = a', b = b', c = c', d = d'. \quad (\text{B4})$$

Hence, the density matrix  $\rho_A^\zeta$  becomes

$$\rho_A^\zeta = \sum_{c,d} \sum_{g \in G, g' \in G_A} \frac{1}{|G|} \sum_{a,b} |\alpha_{ab,cd}|^2 (\eta_2^x)^c (\gamma_2^x)^d g_A |0\rangle_{AA} \langle 0| (\eta_2^{x\dagger})^c (\gamma_2^{x\dagger})^d (g_A g_A')^\dagger. \quad (\text{B5})$$

From this form we obtain

$$\text{Tr}_A[(\rho_A^\zeta)^n] = \sum_{c,d} \left[ \sum_{a,b} |\alpha_{ab,cd}|^2 \right]^n \times \left( \frac{|G_A| |G_B|}{|G|} \right)^{n-1}. \quad (\text{B6})$$

The entanglement entropy is given by

$$S_A = \lim_{n \rightarrow 1} \frac{1}{1-n} \log \text{tr}_A(\rho_A^\zeta)^n = \log \frac{|G|}{|G_A||G_B|} - \sum_{c,d} \left[ \left( \sum_{a,b} |\alpha_{ab,cd}|^2 \right) \log \left( \sum_{a,b} |\alpha_{ab,cd}|^2 \right) \right]. \quad (\text{B7})$$

Therefore, (41) follows.

## 2. Single row II

In the case of Fig. (4)(b), from (23) (see also Fig. 3b), it follows that two logical operators running in the  $y$ -direction,  $\eta_2^x$  and  $\gamma_2^x$  exclusively act on B. Regarding other two,  $\eta_1^x$  and  $\gamma_1^x$  which go around in the  $x$ -direction, one can deform these operators so that they act within A. Therefore the term  $\text{Tr}_B[\dots]$  in (B2) becomes

$$\frac{1}{|G|} \sum_{g,g' \in G} (\eta_1^x)^a (\gamma_1^x)^b g_A |0\rangle_{AA} \langle 0| (g_A g_A')^\dagger (\eta_1^{x\dagger})^{a'} (\gamma_1^{x\dagger})^{b'} \cdot {}_B \langle 0| g_B'^\dagger (\eta_2^x)^{c-c'} (\gamma_2^x)^{d-d'} |0\rangle_B, \quad (\text{B8})$$

from which one finds

$$g_B' = I_B, \quad c = c', d = d'. \quad (\text{B9})$$

The density matrix is then rewritten as

$$\rho_A^\zeta = \sum_{a,b,a',b'} \sum_{c,d} \sum_{g \in G, g' \in G_A} \frac{\alpha_{ab,cd} \bar{\alpha}_{a'b',cd}}{|G|} (\eta_1^x)^a (\gamma_1^x)^b g_A |0\rangle_{AA} \langle 0| (\eta_1^{x\dagger})^{a'} (\gamma_1^{x\dagger})^{b'} (g_A g_A')^\dagger \quad (\text{B10})$$

Introducing orthogonal states by

$$|p, q\rangle_A := \frac{1}{\sqrt{N \times \gcd(N, n_x)}} \sum_{a=0}^{\gcd(n, n_x)-1} \sum_{b=0}^{N-1} \nu^{pa} \omega^{qb} (\eta_1^x)^a (\gamma_1^x)^b |0\rangle_A, \quad (0 \leq p \leq \gcd(N, n_x)-1, 0 \leq q \leq N-1) \quad (\text{B11})$$

with  $\nu = e^{2\pi i / \gcd(N, n_x)}$ ,  $\omega = e^{2\pi i / N}$ , (B10) is transformed as

$$\rho_A^\zeta = \frac{1}{|G|} \sum_{g \in G, g' \in G_A} \sum_{p=0}^{\gcd(N, n_x)-1} \sum_{q=0}^{N-1} \left( \frac{1}{\Gamma} \sigma_{kl} \nu^{kp} \omega^{lq} \right) g_A |p, q\rangle_{AA} \langle p, q| (g_A g_A')^\dagger, \quad (\text{B12})$$

where

$$\sigma_{kl} := \sum_{\substack{a,a',b,b',c,d \\ a-a'=k \pmod{\gcd(N, n_x)} \\ b-b'=l \pmod{N}}} \alpha_{ab,cd} \bar{\alpha}_{a'b',cd}. \quad (\text{B13})$$

Recall that we have defined  $\Gamma = N \times \gcd(N, n_x)$ . Defining  $\lambda_{p,q} := \frac{1}{\Gamma} \sigma_{kl} \nu^{kp} \omega^{lq}$ , we have

$$\text{Tr}_A[(\rho_A^\zeta)^n] = \sum_{p,q} \lambda_{p,q}^n \times \left( \frac{|G_A||G_B|}{|G|} \right)^{n-1}. \quad (\text{B14})$$

Substituting this into

$$S_A = \lim_{n \rightarrow 1} \frac{1}{1-n} \log \text{tr}_A(\rho_A^\zeta)^n \quad (\text{B15})$$

yields (43).

### 3. Single column

In the case of Fig. (4)(c), one can deform the logical operators (23) so that  $\eta_1^x$  and  $\eta_2^x$  act exclusively on B and  $\gamma_2^x$  acts within A, with  $\gamma_1^x$  acting on both of A and B. The term  $\text{Tr}_B[\dots]$  in (B2) is described by

$$\frac{1}{|G|} \sum_{g,g' \in G} (\gamma_{1A}^x)^b (\gamma_2^x)^d g_A |0\rangle_{AA} \langle 0| (g_A g'_A)^\dagger (\gamma_{1A}^{x\dagger})^{b'} (\gamma_2^{x\dagger})^{d'} \cdot {}_B \langle 0| g_B'^\dagger (\eta_1^x)^{a-a'} (\gamma_{1B}^x)^{b-b'} (\eta_2^x)^{c-c'} |0\rangle_B \quad (\text{B16})$$

The inner product gives a constraint

$$g'_B = I_B, \quad a = a', b = b', c = c'. \quad (\text{B17})$$

Define orthogonal states by

$$|b, q\rangle_A := \frac{1}{\sqrt{N}} \sum_{d=0}^{N-1} \omega^{qd} (\gamma_{1A}^x)^b (\gamma_2^x)^d |0\rangle_A, \quad (\text{B18})$$

the density matrix  $\rho_A^\zeta$  is rewritten as

$$\rho_A^\zeta = \frac{1}{|G|} \sum_{g \in G, g' \in G_A} \sum_{b,q} \lambda_q^{(b)} g_A |b, q\rangle_{AA} \langle b, q| (g_A g'_A)^\dagger \quad (\text{B19})$$

with

$$\lambda_q^{(b)} = \frac{1}{N} \sum_{k=0}^{N-1} \omega^{kq} \sigma_k^{(b)}, \quad \sigma_k^{(b)} = \sum_{\substack{a,c,d,d' \\ d-d'=k \pmod{N}}} \alpha_{ab,cd} \bar{\alpha}_{ab,cd'}. \quad (\text{B20})$$

By calculating (B15), one obtains (50).